Environmental Science & Technology

pubs.acs.org/est

Article

Ultrahigh Peroxymonosulfate Utilization Efficiency over CuO Nanosheets via Heterogeneous Cu(III) Formation and Preferential Electron Transfer during Degradation of Phenols

Yan Wei, Jie Miao, Jianxin Ge, Junyu Lang, Chunyang Yu, Lizhi Zhang, Pedro J. J. Alvarez, and Mingce Long*

Cite This: *Environ. Sci. Technol.* 2022, 56, 8984−8992

Read Online

ACCESS | Metrics & More | Article Recommendations | Supporting Information

ABSTRACT: In persulfate activation by copper-based catalysts, high-valent copper (Cu(III)) is an overlooked reactive intermediate that contributes to efficient persulfate utilization and organic pollutant removal. However, the mechanisms underlying heterogeneous activation and enhanced persulfate utilization are not fully understood. Here, copper oxide (CuO) nanosheets (synthesized with a facile precipitation method) exhibited high catalytic activity for peroxymonosulfate (PMS) activation with 100% 4-chlorophenol (4-CP) degradation within 3 min. Evidence for the critical role of surface-associated Cu(III) on PMS activation and 4-CP degradation over a wide pH range (pH 3−10) was obtained using in situ Raman spectroscopy, electron paramagnetic resonance, and quenching tests. Cu(III) directly oxidized 4-CP and other phenolic pollutants, with rate constants inversely proportional to their ionization potentials. Cu(III) preferentially oxidizes 4-CP rather than react with two PMS molecules to generate one molecule of $^1O_2$, thus minimizing this less efficient PMS utilization pathway. Accordingly, a much higher PMS utilization efficiency (77% of electrons accepted by PMS ascribed to 4-CP mineralization) was obtained with CuO/PMS than with a radical pathway-dominated Co_3O_4/PMS system (27%) or with the $^1O_2$ pathway-dominated α-MnO_2/PMS system (26%). Overall, these results highlight the potential benefits of PMS activation via heterogeneous high-valent copper oxidation and offer mechanistic insight into ultrahigh PMS utilization efficiency for organic pollutant removal.

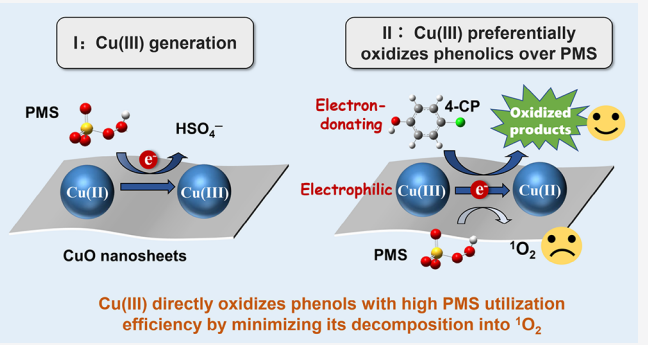

KEYWORDS: *persulfate activation, high-valent copper, oxidant utilization efficiency, heterogeneous catalysis*

1. INTRODUCTION

Persulfate-based advanced oxidation processes (AOPs) have drawn increasing attention to degrade recalcitrant organic pollutants. Persulfate activation (including peroxymonosulfate (PMS) and peroxodisulfate (PDS)) traditionally refers to peroxide bond cleavage through electron- or energy-transferring processes that generate free radicals, including $^{\bullet}OH$ and $SO_4^{\bullet-}$.[1] Owing to the high redox potential of the generated radicals ($E^0(SO_4^{\bullet-}/SO_4^{2-})$ = 2.6−3.1 V_{NHE} and $E^0(^{\bullet}OH/OH^-)$ = 1.9−2.7 V_{NHE}) and their broad reactivity, radical pathway-dominated persulfate activation systems generally exhibit poor selectivity[1] and suffer from extensive radical self-recombination or scavenging by persulfate and background water constituents (e.g., dissolved organic matter, carbonates, Cl^-, and NO_3^-).[2] This leads to low persulfate utilization efficiency and hinders practical application.[3,4] The absence of free radicals in the nonradical pathway of persulfate activation holds promise to enhance the persulfate utilization efficiency.[5] The nonradical pathway generates other reactive species, including metastable persulfate/catalyst complexes,[6,7] singlet oxygen ($^1O_2$),[8,9] and high-valent metals.[10−12] However, our mechanistic understanding of which a nonradical pathway enhances persulfate utilization efficiency is rather limited.

Metastable persulfate/catalyst complexes interact with target pollutants and accept electrons to accomplish oxidation, which mainly takes place at the surface of carbonaceous materials. However, the redox potential of the metastable species is low (0.6−1.2 V), limiting pollutant degradation capabilities.[6] In $^1O_2$-dominated persulfate activation by metal-based catalysts, one mole of $^1O_2$ can be produced by consuming two moles of PMS through cycling the transition metal between low and

Received: March 20, 2022
Revised: May 21, 2022
Accepted: May 23, 2022
Published: May 31, 2022

high valence.[13,14] Furthermore, the contribution of the generated $^1O_2$ to pollutant degradation is limited by its high decay rate in water (2.5×10^5 s^{-1}).[15] Thus, persulfate utilization via the $^1O_2$-based treatment pathway is relatively inefficient. Alternatively, high-valent metal species were recently found to be strong oxidants generated during persulfate activation by metal-containing catalysts.[1,10] These reactive species are produced by consuming only one mole of persulfate and can directly oxidize organic substrates with minimal scavenging, resulting in higher PMS utilization efficiency than other activation pathways.[16,17] For instance, high-valent iron (Fe(IV) and Fe(V)) and cobalt (Co(IV)) have been identified as persulfate activation byproducts when using heterogeneous catalysts such as cellulosic fiber-bonded cobalt phthalocyanine (CFs-CoPc) complex,[18] Fe(III)-doped carbon-based materials,[19,20] and nanoscale zero-valent iron.[21]

High-valent copper (e.g., Cu(III)) can also be generated during persulfate activation, and this strong oxidizing and low toxicity species has been proposed for AOP applications.[22−24] Cu(III) was determined to be the primary intermediate oxidant in homogeneous Cu(II)/PMS[23] and Cu(II)/PDS[22] oxidation. However, homogeneous Cu(III) can only be generated under neutral to slightly alkaline conditions with Cu(II) mainly existing as $Cu(OH)_2$ colloids.[23] Recently, heterogeneous Cu(III) was observed in persulfate catalytic activation by MgO modified CuO/Fe_3O_4[25] and by single-atom catalyst Cu-N_4.[26] Note that the reduction potential of Cu(III)/Cu(II) in an ionized form is 1.57 V, but it increases to 2.3 V in the solid phase, which is even higher than those of high-valent iron (E^0(Fe(VI)) = 2.2 V) and manganese (E^0(Mn(VII)) = 1.68 V).[27,28] Thus, generating high-valent, surface-associated copper in heterogeneous systems is conducive to organic degradation due to its higher oxidative potential.[29] However, the mechanisms of surface-associated Cu(III) generation and high persulfate utilization efficiency for organic pollutant removal are not fully understood.

This paper reports the facile synthesis and application of CuO nanosheets for efficient PMS activation and utilization. The catalytic performance of CuO for PMS activation was evaluated by quantifying PMS decomposition and 4-chlorophenol (4-CP) degradation. In situ Raman spectroscopy and EPR were used to investigate the role of high-valent copper in PMS activation and 4-CP degradation over a wide pH range (pH 3−10). We demonstrate that surface-associated Cu(III) serves as the key reactive species in the mineralization of phenolic compounds and offers novel mechanistic insight into how this pathway leads to ultrahigh PMS utilization efficiency.

2. EXPERIMENTAL SECTION

2.1. Reagents. Details of reagents are listed in Text S1.

2.2. Catalyst Preparation and Characterization. The copper oxide was synthesized by a facile precipitation method. Briefly, 15 mmol of $Cu(NO_3)_2{\cdot}3H_2O$ was dissolved in 20 mL of deionized water. Then, 15 mL of NaOH (4 M) was added dropwise followed by stirring for an extra 2 h at 90 °C. Then, the precipitates were filtered, washed, and calcined at 400 °C for 2 h at a rate of 5 °C min^{-1}. α-MnO_2 was prepared via a previously reported hydrothermal method.[30] The characterization of CuO is described in Text S2.

2.3. Organic Degradation Tests. The catalytic performance of the catalysts was measured by PMS activation for organic degradation. Taking 4-CP degradation as an example, CuO (0.2 g/L) was mixed with 4-CP solution (10 mg/L). After stirring at 25 °C for 30 min to achieve the adsorption and desorption equilibrium, PMS (0.2 mM) was added to initiate the reaction under stirring. At selected time intervals, a precisely measured sample (0.5 mL) was withdrawn and filtered into a high-performance liquid chromatography (HPLC) vial containing 0.5 mL of methanol to quench the reaction.

2.4. Analytical Methods. The concentration of organic pollutants was detected by HPLC (Shimadzu LC-2010AHT), equipped with a Shim Pack C18 chromatographic column (ZORBAX Eclipse XDB-C18) and a UV−vis detector (SPD-20AV). Detailed HPLC analytical conditions are listed in Table S1. The intermediates of 4-CP degradation were determined by ultraperformance liquid chromatography/quadrupole-time-of-flight mass-spectrometry (UPLC/QTOF-MS, Acquity UPLC/QTOF Premier, Waters). The residual PMS concentration was determined by an ABTS method.[31] Each test was conducted in triplicate. Data represent mean values and error bars corresponding to standard deviations. Statistical analysis was evaluated by Student's paired *t*-test (single-tailed) with a significance limit of 5%.

The concentrations of CO_2 generated during 4-CP mineralization and O_2 generated during PMS decomposition were determined in airtight bottles by gas chromatography (Shimadzu GC-14B) and a fiber-optic oxygen transmitter (Planar Oxygen-Sensitive Spot, SP-PSt7-10-NAU-D5-YOP, PreSens Precision Sensing GmbH), respectively.

PMS utilization efficiency is generally assessed by calculating Δ[target pollutant]/Δ[PMS].[32,33] However, this approach has significant limitations since it fails to distinguish different extents of organic degradation (e.g., partial degradation versus mineralization to CO_2 and water). Herein, we considered the ratio of the amount of PMS used for 4-CP mineralization ($n_{PMS,\ mineralization}$, mol, assessed per CO_2 production) to the amount of PMS decomposed ($n_{PMS,\ decomposition}$, mol) to evaluate PMS utilization efficiency for 4-CP mineralization (PUE). Although the PUE value ignores PMS consumption by formation of byproducts of incomplete 4-CP mineralization (which could not be precisely quantified), it accurately appraises PMS utilization for complete degradation compared with the Δ[target pollutant]/Δ[PMS] value, thus effectively evaluating the mineralization ability of different AOP systems. PUE was calculated based on stoichiometric considerations as follows (eq 1), where n_{CO_2} is the measured amount of CO_2 (mol) evolved from 4-CP mineralization and $n_{PMS,\ decomposition}$ is the number of moles of PMS consumed, with additional details provided in Text S3.

$$\mathrm{PUE} = \frac{13(n_{CO_2})}{6(n_{PMS,decomposition})} \quad (1)$$

2.5. Theoretical Calculations. Details of theoretical calculations are provided in Text S4.

3. RESULTS AND DISCUSSION

3.1. Catalytic Performance of CuO for PMS Activation. SEM and TEM images show that CuO exhibits a nanosheet microstructure with a thickness of about 25 nm (Figure 1a), which contributes to a relatively high specific surface area (18.2 m^2/g; Figure S1a). An interplanar spacing of 0.25 nm corresponds to the (−111) plane of CuO. The XRD

https://doi.org/10.1021/acs.est.2c01968
Environ. Sci. Technol. 2022, 56, 8984−8992

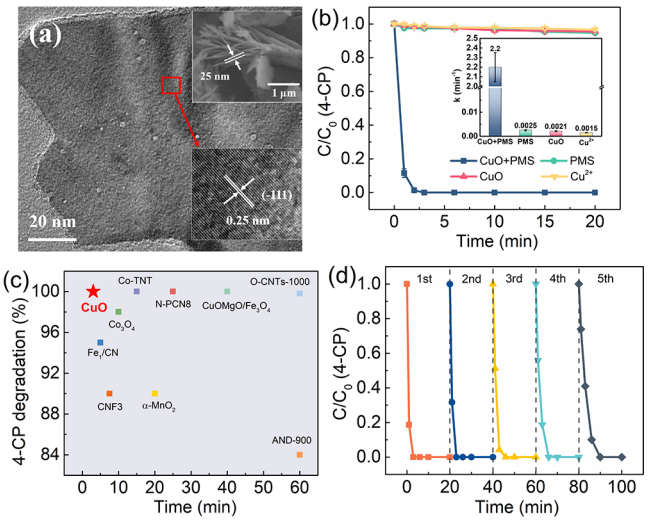

Figure 1. (a) TEM image of CuO (insets are SEM and HRTEM images); (b) 4-CP degradation in different systems; (c) comparison of 4-CP degradation in various PMS activation systems; (d) cycle tests showing stable 4-CP degradation in the CuO/PMS system. Conditions: $[4\text{-CP}]_0$ = 10 mg/L, [catalyst] = 0.2 g/L, [PMS] = 0.2 mM, initial pH = 7.0.

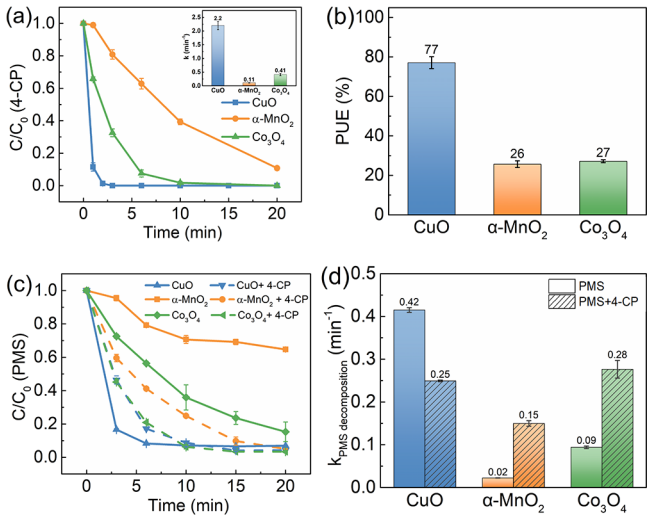

Figure 2. (a) 4-CP degradation in systems with different metal oxide-activated PMS; (b) PUE of different metal oxide/PMS systems; (c) PMS decomposition by different catalysts with or without 4-CP and (d) corresponding PMS decomposition rate constants. Conditions: $[4\text{-CP}]_0$ = 10 mg/L (a, b) or 25 mg/L (c, d), [catalyst] = 0.2 g/L, [PMS] = 0.2 mM, initial pH = 7.0.

pattern corroborated the crystal structure of monoclinic CuO (JCPDS no. 45-0937) (Figure S1b).

The catalytic performance of CuO for PMS activation was evaluated by 4-CP degradation (Figure 1b). Neither CuO nor PMS alone removed significant amounts of 4-CP within 20 min (4 and 5%, respectively). In contrast, combining CuO and PMS resulted in 100% removal of 4-CP in 3 min, with a rate constant of 2.2 ± 0.15 min^{-1}. To exclude the possibility of homogeneous PMS activation by leached copper ions, Cu^{2+} with the same concentration as the Cu in CuO (0.13 g/L) was tested for 4-CP degradation. Cu^{2+} played an imperceptible role in 4-CP removal with only 3% degradation in 20 min. The low PMS activation ability of Cu^{2+} under neutral conditions (the initial pH is about 7.0 in this work) is consistent with previous reports.[23] The above results confirm the ultrahigh catalytic activity of CuO for heterogeneous PMS activation (Figure 1c, details in Table S2 and Figure S2).[3,19,25,34−37] In addition to PMS, CuO can also activate PDS and H_2O_2 to remove 4-CP, but the degradation efficiency was lower than those of PMS (41 and 7% in 20 min, respectively; Figure S3). Apparently, the symmetric structure of PDS makes it more stable and exerts higher steric hindrance than PMS, while the higher bond energy of O−O in H_2O_2 hinders its cleavage.[1] CuO also exhibited a stable and durable catalytic performance in repeated cyclic 4-CP degradation experiments (Figure 1d), and the XRD pattern of the catalyst after five reaction cycles showed negligible change (Figure S4).

3.2. Ultrahigh PMS Utilization Efficiency for 4-CP Mineralization in CuO System. The catalytic performance of CuO was further compared with those of two commonly used metal oxides, α-MnO_2 and Co_3O_4 (characterized by XRD; Figure S5). As shown in Figure 2a, CuO yielded a much higher 4-CP degradation rate constant (2.2 ± 0.15 min^{-1}) than α-MnO_2 (0.11 ± 0.01 min^{-1}) and Co_3O_4 (0.41 ± 0.04 min^{-1}). PUE was proposed to characterize the mineralization performance of the PMS activation system, which reflects the utilization efficiency of decomposed PMS to completely oxidize 4-CP to CO_2. The PUE values of different catalysts are calculated from the measured CO_2 production and PMS consumption (Figure S6). As shown in Figure 2b, CuO displayed an ultrahigh PUE value of 77 ± 3.0%, indicating that 77% of the consumed PMS was coupled to 4-CP mineralization. Compared with CuO, α-MnO_2 and Co_3O_4 exhibited a much lower PMS utilization ability, with PUE values of 26 ± 1.7 and 27 ± 0.7%, respectively.

The role of CuO in the PMS activation pathway was further examined by PMS decomposition with or without 4-CP. To avoid confounding effects by decomposition of residual PMS after 4-CP was completely degraded, the 4-CP concentration was increased to 25 mg/L; this precludes complete 4-CP removal within 20 min (Figure S7). As shown in Figure 2c,d, in the absence of 4-CP, all three metal oxides can induce PMS decomposition, with decomposition rate constants of 0.42 ± 0.006 min^{-1} for CuO, 0.02 ± 0.001 min^{-1} for α-MnO_2, and 0.09 ± 0.003 min^{-1} for Co_3O_4. With the addition of 4-CP (25 mg/L), the rate constant for PMS decomposition by CuO decreased significantly to 0.25 ± 0.002 min^{-1}. In contrast, in α-MnO_2/PMS and Co_3O_4/PMS systems, 4-CP accelerated PMS decompositions to 0.15 ± 0.006 and 0.28 ± 0.021 min^{-1}, respectively. Apparently, 4-CP retards CuO-catalyzed PMS decomposition because CuO activates PMS by a different pathway from those of α-MnO_2 and Co_3O_4. PMS activation by α-MnO_2 proceeds via $^1O_2$,[38] while activation by Co_3O_4 involves a radical pathway.[39] This was verified by quenching and solvent substitution experiments (Figure S8). Therefore, we postulate that the degradation of 4-CP in CuO/PMS is dominated by a different activation pathway that results in highly efficient PMS utilization.

3.3. Cu(III) Enhances PMS Utilization by Minimizing Its Decomposition into $^1O_2$ during Phenol Degradation. To discern the underlying mechanism that contributes to the ultrahigh PUE, we examined the PMS activation pathway (including $^1O_2$ generation) in the CuO/PMS system. As shown in Figure 3a, the PMS concentration briskly decreased with CuO addition in the absence of organics, even when the initial concentration was as high as 2 mM. The decomposition

https://doi.org/10.1021/acs.est.2c01968
Environ. Sci. Technol. 2022, 56, 8984−8992

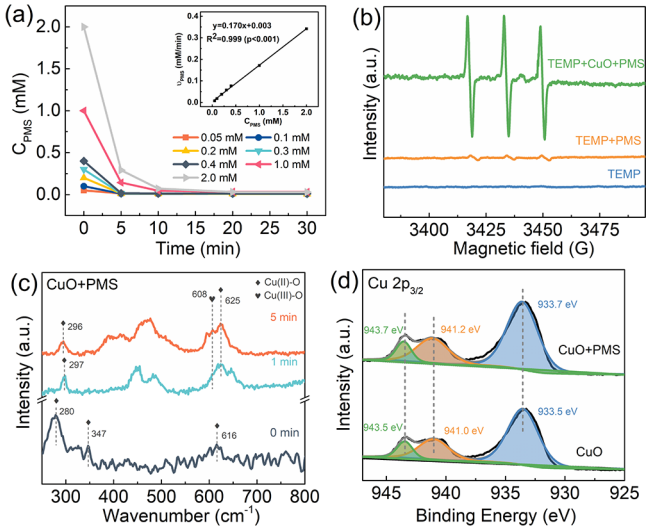

Figure 3. (a) PMS decomposition on the CuO surface in the absence of 4-CP, (b) TEMP spin-trapping EPR spectra of PMS activation in the absence of 4-CP; (c) in situ Raman spectra of CuO after the addition of PMS at varying reaction times; (d) Cu $2p_{3/2}$ XPS spectra of CuO before and after PMS addition. Conditions: [catalyst] = 0.2 g/L, [PMS] = 0.2 mM, initial pH = 7.0.

rate of PMS was linearly related to the PMS concentration (R^2 = 0.999, $p < 0.001$), indicating that PMS decomposition on the CuO surface conforms to the first-order reaction kinetics with a rate constant of 0.17 min^{-1}. Figure 3b shows a strong EPR signal of TEMP-$^1O_2$. After the introduction of CuO, the dissolved oxygen concentration of the CuO/PMS system increased significantly (Figure S9), which originated from the unproductive decay of $^1O_2$ in water. The conversion efficiency of PMS to oxygen catalyzed by CuO was roughly calculated to be about 80% (Text S5). This infers that $^1O_2$ was the main ROS from PMS decomposition.

In situ Raman spectroscopy analyses were conducted to further unveil the $^1O_2$ generation process during PMS activation over CuO. The Raman spectra of CuO show three peaks at 280, 347, and 616 cm^{-1}, which are characteristic signals of the Cu(II)−O bond (Figure 3c).[40,41] One minute after the addition of PMS alone, a peak at 625 cm^{-1} appeared, which also represents the Cu(II) species.[42] Simultaneously, a weak signal located at 608 cm^{-1} was observed, corresponding to the Cu(III) species.[43] After PMS was added for 5 min, the peak at 608 cm^{-1} became more obvious, suggesting the formation of Cu(III) during the decomposition of PMS by CuO.[44] The electron-donating role of CuO was further ascertained by XPS. As shown in Figure 3d, the peaks at the binding energies of 943.5 and 941.0 eV represent satellite peaks of Cu(II). The Cu $2p_{3/2}$ peak of fresh CuO was located at 933.5 eV, suggesting that Cu(II) is the dominant Cu species.[45,46] After the addition of PMS, the binding energy of Cu $2p_{3/2}$ shifted to a higher position (933.7 eV). This implies an increase in the Cu(II) valence state during PMS decomposition, which corroborates the in situ Raman spectra.

These data infer a Cu(III)-induced PMS decomposition pathway in the absence of organics. With the addition of PMS, a metastable ≡Cu(II)···O(OH)—SO_3^-···Cu(II)≡ intermediate is generated (eq 2). Then, rapid electron transfer occurs in this intermediate, resulting in the breakage of the O−O bond and the generation of ≡Cu(III)—O—Cu(III)≡ species, which is similar to the structure of high-valent Cu(III) bis-μ-oxo species (step I, eq 3).[43,47] The reactive ≡Cu(III)—O—Cu(III)≡ undergoes nucleophilic attack by other HSO_5^- forming $SO_5^{\bullet-}$ (step II, eq 4). Finally, $SO_5^{\bullet-}$ undergoes rapid self-recombination to generate $^1O_2$ (step III, eq 5).

$$2 \equiv Cu(II) + HSO_5^- \rightarrow \equiv Cu(II)\cdots O(OH) - SO_3^- \cdots Cu(II) \equiv \quad (2)$$

$$\equiv Cu(II)\cdots O(OH) - SO_3^- \cdots Cu(II) \equiv \rightarrow \equiv Cu(III) - O - Cu(III) \equiv + HSO_4^- \quad (3)$$

$$\equiv Cu(III) - O - Cu(III) \equiv + 2HSO_5^- \rightarrow 2 \equiv Cu(II) + 2SO_5^{\bullet-} + H_2O \quad (4)$$

$$2SO_5^{\bullet-} \rightarrow S_2O_8^{2-} + {}^1O_2 \quad (5)$$

Generally, the presence of organic pollutants increases PMS decomposition by promoting ROS generation.[4,48] However, the intensity of TEMO-$^1O_2$ signals decreased in the presence of 4-CP (Figure 4a). The lower $^1O_2$ concentration can be

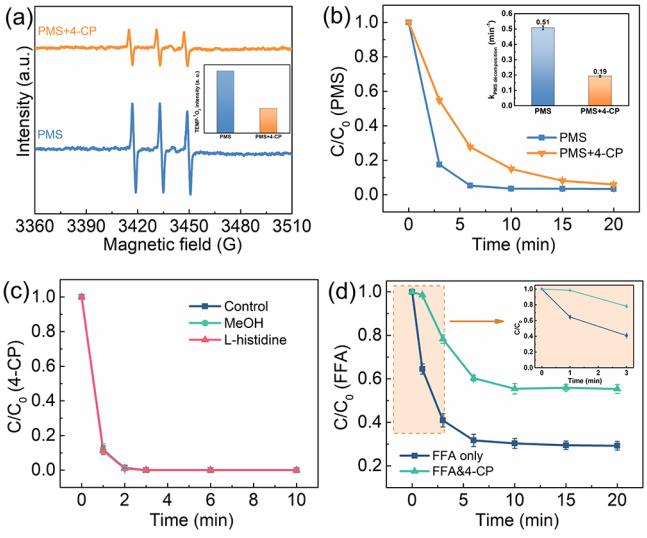

Figure 4. (a) TEMP spin-trapping EPR spectra of PMS activation with or without 4-CP (inset: the corresponding TEMO-$^1O_2$ signal intensity for the two systems); (b) PMS decomposition on CuO with or without 4-CP; (c) effect of quencher on 4-CP degradation; (d) effect of coexisting 4-CP on FFA degradation. Conditions: $[organics]_0$ = 10 mg/L, [catalyst] = 0.2 g/L, [PMS] = 0.2 mM, [TEMP] = 5 mM, [MeOH] = 200 mM, [L-histidine] = 5 mM, initial pH = 7.0.

ascribed to either decreased $^1O_2$ generation or accelerated $^1O_2$ consumption. However, 4-CP slowed down PMS decomposition over CuO from 0.51 ± 0.01 to 0.19 ± 0.01 min^{-1} (Figure 4b), suggesting decreased $^1O_2$ generation. Furthermore, L-histidine, a $^1O_2$ quencher, did not significantly suppress 4-CP removal (Figure 4c), and the substitution of D_2O for H_2O cannot accelerate 4-CP degradation (Figure S10), corroborating that $^1O_2$ played an insignificant role in 4-CP degradation.[35] FFA (a common probe of $^1O_2$) exhibited an expected two-stage degradation in the presence of 4-CP (Figure 4d). FFA removal was significantly inhibited in the first minute (only 1% within 1 min) until 4-CP was completely removed, and then, FFA was gradually degraded by the remaining PMS. However, 4-CP degradation was virtually

https://doi.org/10.1021/acs.est.2c01968
Environ. Sci. Technol. 2022, 56, 8984−8992

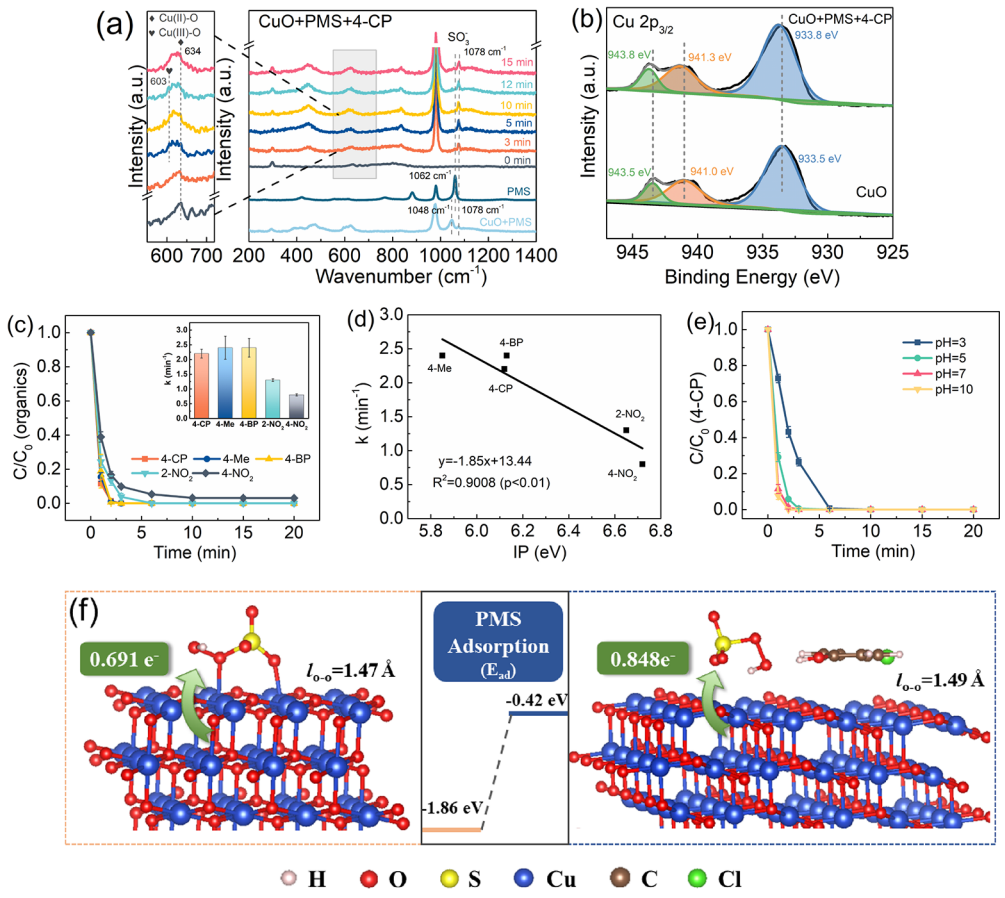

Figure 5. (a) In situ Raman spectra of CuO after the addition of PMS and 4-CP; (b) Cu $2p_{3/2}$ XPS spectra of CuO before and after 4-CP degradation; (c) degradation of different phenolic compounds by CuO-activated PMS; (d) relationship between k_{obs} and the ionization potential values of different phenolic compounds; (e) the effect of the initial pH on 4-CP degradation; (f) illustration of the interaction of CuO surfaces with a PMS with/without 4-CP. Conditions: $[organics]_0$ = 10 mg/L, [catalyst] = 0.2 g/L, [PMS] = 0.2 mM, initial pH = 7.0.

unaffected by coexisting FFA (Figure S11). The rate constant of FFA and $^1O_2$ ($k_{FFA,\ ^1O_2}$ = 1.2 × 10^8 $M^{-1}s^{-1}$) is 2 orders of magnitude higher than that of 4-CP ($k_{4\text{-}CP,\ ^1O_2}$ = 6.0 × 10^6 $M^{-1}s^{-1}$), indicating a minor contribution of $^1O_2$ to 4-CP degradation.[15,49] Overall, these data infer that the decreased $^1O_2$ concentration in the CuO/PMS system during 4-CP degradation was due to lower $^1O_2$ generation instead of accelerated $^1O_2$ consumption by 4-CP.

A rough calculation also eliminates the possibility of $^1O_2$ being predominantly consumed by 4-CP in the CuO/PMS system. The fraction of $^1O_2$ reacting with 4-CP ($f_{^1O_2,4\text{-}CP}$) was calculated in eq 6, where $k_{H_2O,\ ^1O_2}$ is the rate constant for $^1O_2$ quenching by water (2.5 × 10^5 s^{-1})[50]

$$f_{^1O_2,4\text{-}CP} = \frac{k_{4\text{-}CP,^1O_2}[4\text{-CP}]}{k_{H_2O,^1O_2} + k_{4\text{-}CP,^1O_2}[4\text{-CP}]} \quad (6)$$

The calculated $f_{^1O_2,4\text{-}CP}$ value was 0.186%, inferring that, even if all of the decomposed PMS (94% according to Figure 4b) turned into $^1O_2$, only 0.18 μM $^1O_2$ was utilized for 4-CP degradation in 20 min. However, 78 μM (10 mg/L) 4-CP was removed in 3 min, suggesting that 4-CP was degraded via a non-$^1O_2$ dominated pathway. Apparently, the suppression of $^1O_2$ generation (and subsequent unproductive consumption) during 4-CP degradation was conducive to ultrahigh PUE during 4-CP degradation.

To determine the organic degradation mechanism that results in ultrahigh PUE, the contribution of radicals to 4-CP degradation in PMS activation by CuO was evaluated by scavenging tests. As a scavenger for $^{\bullet}OH$ and $SO_4^{\bullet-}$, MeOH did not significantly inhibit 4-CP degradation even when its concentration was 1000 times that of PMS (Figure 4c). This indicates a limited contribution of $^{\bullet}OH$ and $SO_4^{\bullet-}$ in the CuO/PMS system for pollutant degradation, which is consistent with the low nitrobenzene (NB) degradation capability (Figure S12). Neocuproine (a screening agent for surface Cu(I), which is the intermediate of the inner-sphere electron transfer reaction from adsorbed phenol to CuO[51]) did not significantly affect 4-CP degradation (Figure S13), suggesting that Cu(I) and direct electron transfer from 4-CP to CuO are negligible in this CuO/PMS system. On the other hand, rapid PMS decomposition in the absence of 4-CP excludes PMS activation via formation of CuO surface-activated PMS complexes as oxidizing intermediates.[6,52] Therefore, the contributions from free radicals, $^1O_2$, Cu(I), and surface PMS complexes to organic degradation are negligible in the CuO/PMS system.

We also evaluated Cu(III)-mediated 4-CP oxidation. The involvement of high-valent copper is suggested by the in situ Raman spectra of CuO after the addition of PMS and 4-CP (Figure 5a). After adding PMS to initiate the reaction, the band representing the Cu(II) species (634 cm^{-1}) was gradually broadened in the first 3 min. After 5 min of the reaction, a new

https://doi.org/10.1021/acs.est.2c01968
Environ. Sci. Technol. 2022, 56, 8984−8992

peak located at 603 cm^{-1} was observed, which also represents the Cu(III) species.[40,43,53] As the reaction progresses, the intensity of the peak located at 603 cm^{-1} gradually decreased since the unstable Cu(III) reverted to Cu(II), ensuring the stability of the catalyst. Moreover, the peak located at 1062 cm^{-1} corresponds to the stretching vibrations of SO_3 in PMS (H−O−O−SO_3^-).[7] This SO_3 peak shifted to 1078 cm^{-1} after a 15 min 4-CP degradation, which is ascribed to the enhanced electron density, indicating the electron transfer from CuO to PMS. In contrast, the characteristic peak of SO_3 splits into two peaks (1048 and 1078 cm^{-1}) in CuO/PMS without 4-CP addition. This suggests that, without 4-CP, PMS serves both as an electron acceptor (for Cu(III) generation) and as electron donor (for $^1O_2$ production).[54] This is consistent with the $^1O_2$ generation mechanism discussed above (eqs 2−5). The XPS spectra of the Cu $2p_{3/2}$ peak exhibited a redshift to 933.8 eV after 4-CP degradation, further suggesting the decreased electron density on Cu sites during 4-CP removal (Figure 5b). As a typical one-electron oxidant, Cu(III) is incapable of converting PMSO to $PMSO_2$ via the oxygen transfer pathway as other high-valent metal-oxo species do.[55] The significant contribution of Cu(III) in the CuO/PMS system was indicated by the efficient PMSO oxidation in the presence of NB, a scavenger of $^{\bullet}OH$ (Figure S14).

The intermediates during 4-CP degradation were determined by UPLC-MS analysis (Figure S15a−d), and the main 4-CP degradation pathways by CuO-catalyzed PMS are described in Figure S15e. Two pathways exist in the CuO/PMS system. One way is high-valent copper-initiated carbon-hydrogen bond oxidation with the generation of small molecules eventually mineralized to CO_2, which is similar to the intermediates in radical and Fe(V)-dominated systems.[19,56,57] Another pathway for 4-CP degradation is to form phenolic polymers via single-electron transfer (SET) since Cu(III) is a one-electron oxidant, which may be further mineralized in the CuO/PMS system.[49,51,58]

The structure−activity relationship for organic degradation in the Cu(III)-mediated CuO/PMS system was also investigated. In the SET mechanism dominated nonradical reaction of PMS activation, the degradation rates of organics depend greatly on the electron-donating ability of organics,[28] which can be described by ionization potential (IP, eV).[59] Five different phenolic compounds were tested as target pollutants, and the relationship between the degradation rate constant (k_{obs}, min^{-1}) and IP of different organics (data from our previous work[59]) was explored. As shown in Figure 5c, all five phenolic compounds were efficiently removed, but nitrophenols (2-NO_2 and 4-NO_2) were degraded slower ($k_{2\text{-}NO2}$ = 1.3 ± 0.04 min^{-1} and $k_{4\text{-}NO2}$ = 0.8 ± 0.04 min^{-1}). An inversely linear relationship between IP and k_{obs} was obtained (Figure 5d), suggesting that the electron-donating ability of organics, a determinant of a rate-limiting SET mechanism, notably affects the preferential reaction of the CuO/PMS system. The underlying basis for this affinity can be ascribed to the electrophilicity of Cu(III) species, leading to its higher affinity for phenols with stronger electron-donating ability.[60,61] The IP of PMS was calculated to be 7.7 eV, even higher than 4-nitrophenol (6.7 eV). Therefore, Cu(III) species preferentially oxidizes phenols instead of PMS, contributing to the less PMS consumption.

Compared with the narrow low-pH requirement of homogeneous Cu(III) oxidation,[23,62] heterogeneous Cu(III) exhibits superior oxidation activity over a wide pH range. As shown in Figure 5e, 4-CP was 100% degraded within 6 min at the initial pH varying from 3 to 10. The marginally sluggish 4-CP degradation at pH = 3 can be attributed to the intensified Cu^{2+} leaching, which is detrimental to the heterogeneous catalysis. The wide pH range of the CuO/PMS system makes it promising for practical application. Moreover, the non-enhancement of 4-CP degradation under alkaline conditions further demonstrates that $^1O_2$ is not the main reactive species contributing to 4-CP degradation since the rate of singlet oxygenation of phenolic compounds increases with increasing pH.[63]

Density functional theory (DFT) calculations further corroborate Cu(III)-induced PMS activation in the CuO/PMS system. The reaction pathway with the corresponding relative energy profile is shown in Figure S16. The negative ΔG of ≡Cu(III)—O—Cu(III)≡ generation (−0.11 eV) suggests that the PMS decomposition on the surface of CuO (eqs 2 and 3) is thermodynamically favorable. In addition, in the absence of 4-CP, strong PMS adsorption is observed with an adsorption energy (E_{ad}) of −1.86 eV (Figure 5f) in the initial step, and CuO serves as the electron donor for PMS decomposition and the calculated number of electrons transferred (Q) is 0.691 e. After the addition of 4-CP, the adsorption energy of PMS is significantly decreased to −0.42 eV, while the calculated total number of electrons transferred to PMS increases to 0.848 e, and the peroxide bond length in PMS becomes longer. This suggests that the presence of 4-CP enhances PMS electron-accepting ability and favors its activation to produce Cu(III). The weakening PMS adsorption on the surface of CuO also explains the slowing down of PMS decomposition in the presence of 4-CP (Figure 4b).

Heterogeneous Cu(III)-dominated PMS activation for 4-CP degradation is illustrated in the TOC image. In summary, the reaction is triggered by the oxidation of CuO by PMS to produce reactive ≡Cu(III)—O—Cu(III)≡ (eqs 2 and 3). Then, the generated electrophilic ≡Cu(III)—O—Cu(III)≡ species directly and preferentially oxidizes 4-CP due to its lower redox potential ($E_{1/2(4\text{-}CP)}$ = 0.9 V < $E^0(HSO_5^-/SO_5^{\bullet-})$ = 1.1 V) and IP ($IP_{4\text{-}CP}$ = 6.1 eV < IP_{PMS} = 7.7 eV) than PMS.[1,23,59] As a result, wasteful $^1O_2$ generation is mitigated, resulting in the ultrahigh PUE for 4-CP degradation.

4. ENVIRONMENTAL IMPLICATIONS

This work developed a method for highly efficient PMS activation and utilization for phenol degradation using CuO nanosheets as catalysts and surface-associated Cu(III) species as oxidants. Unlike the radical-dominated (e.g., Co_3O_4/PMS) or $^1O_2$-dominated (e.g., MnO_2/PMS) systems, oxidation of organic pollutants by Cu(III) can avoid wasteful consumption of PMS by radicals and quenching of $^1O_2$ by water. Importantly, the generated electrophilic Cu(III) species preferentially reacts with electron-rich phenolic compounds rather than with PMS, thus minimizing the relatively inefficient $^1O_2$-dominated 4-CP degradation pathway. This explains the high PMS utilization efficiency observed in high-valent metal-dominated pollutant degradation systems.

Compared with the pH-limited homogeneous Cu^{3+} oxidation, heterogeneous Cu(III) exhibits superior oxidation capability over a wide pH range (from pH 3 to 10). The electrophilic characteristics of Cu(III) are conducive to direct and efficient degradation of aromatic pollutants whose high electron-donating propensity (reflected by high ionization potential) minimizes wasteful consumption of surface-

https://doi.org/10.1021/acs.est.2c01968
Environ. Sci. Technol. 2022, 56, 8984−8992

associated Cu(III) by background water constituents and contributes to high PMS utilization efficiency. Thus, this CuO/PMS system is promising for removal of priority aromatic pollutants in complex wastewater matrices.

Overall, this work advances mechanistic understandings of heterogeneous Cu(III)-associated persulfate activation and provides novel insights into the underlying reason for ultrahigh PMS utilization efficiency in high-valent metal-dominated systems during aromatic pollutant removal.

■ ASSOCIATED CONTENT

Supporting Information

The Supporting Information is available free of charge at https://pubs.acs.org/doi/10.1021/acs.est.2c01968.

Reagents (Text S1), catalyst characterization (Text S2), PUE calculation method (Text S3), theoretical calculation (Text S4), PMS conversion to $^1O_2$ (Text S5), HPLC conditions (Table S1), catalytic performance of catalysts (Table S2 and Figure S2), adsorption isotherms and XRD patterns (Figures S1, S4, and S5), effect of oxidants (Figure S3), catalysts (Figure S7), solvents (Figure S10), FFA (Figure S11), and neocuproine (Figure S13), CO_2 production and PMS consumption (Figure S6), reactive species in Co_3O_4 and MnO_2 systems (Figure S8), dissolved oxygen evolution (Figure S9), NB and PMSO oxidation (Figure S12 and S14), UPLC-MS chromatogram (Figure S15), and relative Gibbs free energy of Cu(III) formation (Figure S16) (PDF)

■ AUTHOR INFORMATION

Corresponding Author

Mingce Long − *School of Environmental Science and Engineering, Key Laboratory for Thin Film and Microfabrication of the Ministry of Education, Shanghai Jiao Tong University, Shanghai 200240, China;* orcid.org/0000-0002-5168-8330; Phone: 86-21-54747354; Email: long_mc@sjtu.edu.cn; Fax: 86-21-54740825

Authors

Yan Wei − *School of Environmental Science and Engineering, Key Laboratory for Thin Film and Microfabrication of the Ministry of Education, Shanghai Jiao Tong University, Shanghai 200240, China*

Jie Miao − *School of Environmental Science and Engineering, Key Laboratory for Thin Film and Microfabrication of the Ministry of Education, Shanghai Jiao Tong University, Shanghai 200240, China*

Jianxin Ge − *School of Environmental Science and Engineering, Key Laboratory for Thin Film and Microfabrication of the Ministry of Education, Shanghai Jiao Tong University, Shanghai 200240, China*

Junyu Lang − *School of Physical Science and Technology, Shanghai Tech University, Shanghai 201210, China*

Chunyang Yu − *School of Chemistry and Chemical Engineering, Shanghai Jiao Tong University, Shanghai 200240, China;* orcid.org/0000-0003-1175-8362

Lizhi Zhang − *School of Environmental Science and Engineering, Key Laboratory for Thin Film and Microfabrication of the Ministry of Education, Shanghai Jiao Tong University, Shanghai 200240, China;* orcid.org/0000-0002-6842-9167

Pedro J. J. Alvarez − *Department of Civil and Environmental Engineering, Rice University, Houston, Texas 77005, United States;* orcid.org/0000-0002-6725-7199

Complete contact information is available at: https://pubs.acs.org/10.1021/acs.est.2c01968

Notes

The authors declare no competing financial interest.

■ ACKNOWLEDGMENTS

Financial support from the National Natural Science Foundation of China (nos. 21876108, 22106104, 22111530110, and 52070128), the National Institute of Environmental Health Sciences of the National Institutes of Health, USA (no. P42ES027725), and NSF ERC on Nanotechnology-Enabled Water Treatment (EEC-1449500) is gratefully acknowledged.

■ REFERENCES

(1) Lee, J.; von Gunten, U.; Kim, J.-H. Persulfate-based advanced oxidation: Critical assessment of opportunities and roadblocks. *Environ. Sci. Technol.* **2020**, *54*, 3064−3081.

(2) Duan, X.; Sun, H.; Shao, Z.; Wang, S. Nonradical reactions in environmental remediation processes: Uncertainty and challenges. *Appl. Catal., B* **2018**, *224*, 973−982.

(3) Zhang, L.-S.; Jiang, X.-H.; Zhong, Z.-A.; Tian, L.; Sun, Q.; Cui, Y.-T.; Lu, X.; Zou, J.-P.; Luo, S.-L. Carbon nitride supported high-loading fe single-atom catalyst for activating of peroxymonosulfate to generate $^1O_2$ with 100% selectivity. *Angew. Chem., Int. Ed.* **2021**, *60*, 21751−21755.

(4) Huang, K. Z.; Zhang, H. Direct electron-transfer-based peroxymonosulfate activation by iron-doped manganese oxide (δ-MnO_2) and the development of galvanic oxidation processes (GOPs). *Environ. Sci. Technol.* **2019**, *53*, 12610−12620.

(5) Ren, W.; Xiong, L.; Nie, G.; Zhang, H.; Duan, X.; Wang, S. Insights into the electron-transfer regime of peroxydisulfate activation on carbon nanotubes: The role of oxygen functional groups. *Environ. Sci. Technol.* **2020**, *54*, 1267−1275.

(6) Ren, W.; Cheng, C.; Shao, P.; Luo, X.; Zhang, H.; Wang, S.; Duan, X. Origins of electron-transfer regime in persulfate-based nonradical oxidation processes. *Environ. Sci. Technol.* **2022**, *56*, 78−97.

(7) Ren, W.; Nie, G.; Zhou, P.; Zhang, H.; Duan, X.; Wang, S. The intrinsic nature of persulfate activation and N-doping in carbocatalysis. *Environ. Sci. Technol.* **2020**, *54*, 6438−6447.

(8) Gao, Y.; Wu, T.; Yang, C.; Ma, C.; Zhao, Z.; Wu, Z.; Cao, S.; Geng, W.; Wang, Y.; Yao, Y.; Zhang, Y.; Cheng, C. Activity trends and mechanisms in peroxymonosulfate-assisted catalytic production of singlet oxygen over atomic metal-N-C catalysts. *Angew. Chem., Int. Ed.* **2021**, *60*, 22513−22521.

(9) Mi, X.; Wang, P.; Xu, S.; Su, L.; Zhong, H.; Wang, H.; Li, Y.; Zhan, S. Almost 100% peroxymonosulfate conversion to singlet oxygen on single-atom CoN_{2+2} sites. *Angew. Chem., Int. Ed.* **2021**, *60*, 4588−4593.

(10) Zong, Y.; Guan, X.; Xu, J.; Feng, Y.; Mao, Y.; Xu, L.; Chu, H.; Wu, D. Unraveling the overlooked involvement of high-valent cobalt-oxo species generated from the cobalt(II)-activated peroxymonosulfate process. *Environ. Sci. Technol.* **2020**, *54*, 16231−16239.

(11) Wang, Z.; Jiang, J.; Pang, S.; Zhou, Y.; Guan, C.; Gao, Y.; Li, J.; Yang, Y.; Qiu, W.; Jiang, C. Is sulfate radical really generated from peroxydisulfate activated by iron (II) for environmental decontamination? *Environ. Sci. Technol.* **2018**, *52*, 11276−11284.

(12) Wang, Z.; Qiu, W.; Pang, S.-Y.; Guo, Q.; Guan, C.; Jiang, J. Aqueous iron(IV)-oxo complex: An emerging powerful reactive oxidant formed by iron(II)-based advanced oxidation processes for oxidative water treatment. *Environ. Sci. Technol.* **2022**, *56*, 1492−1509.

(13) Mi, X.; Zhong, H.; Zhang, H.; Xu, S.; Li, Y.; Wang, H.; Zhan, S.; Crittenden, J. C. Facilitating redox cycles of copper species by pollutants in peroxymonosulfate activation. *Environ. Sci. Technol.* **2022**, *56*, 2637−2646.
(14) Evans, D. F.; Upton, M. W. Studies on singlet oxygen in aqueous solution. Part 3. The decomposition of peroxy-acids. *Dalton Trans.* **1985**, *6*, 1151−1153.
(15) Wilkinson, F.; Helman, W. P.; Ross, A. B. Rate constants for the decay and reactions of the lowest electronically excited singlet state of molecular oxygen in solution. An expanded and revised compilation. *J. Phys. Chem. Ref. Data* **1995**, *24*, 663−677.
(16) Gao, Y.; Zhou, Y.; Pang, S. Y.; Jiang, J.; Shen, Y. M.; Song, Y.; Duan, J. B.; Guo, Q. Enhanced peroxymonosulfate activation via complexed Mn(II): A novel non-radical oxidation mechanism involving manganese intermediates. *Water Res.* **2021**, *193*, No. 116856.
(17) Chen, F.; Liu, L. L.; Chen, J. J.; Li, W. W.; Chen, Y. P.; Zhang, Y. J.; Wu, J. H.; Mei, S. C.; Yang, Q.; Yu, H. Q. Efficient decontamination of organic pollutants under high salinity conditions by a nonradical peroxymonosulfate activation system. *Water Res.* **2021**, *191*, No. 116799.
(18) Huang, Z.; Yao, Y.; Lu, J.; Chen, C.; Lu, W.; Huang, S.; Chen, W. The consortium of heterogeneous cobalt phthalocyanine catalyst and bicarbonate ion as a novel platform for contaminants elimination based on peroxymonosulfate activation. *J. Hazard. Mater.* **2016**, *301*, 214−221.
(19) Li, H.; Shan, C.; Pan, B. Fe(III)-doped g-C_3N_4 mediated peroxymonosulfate activation for selective degradation of phenolic compounds via high-valent iron-oxo species. *Environ. Sci. Technol.* **2018**, *52*, 2197−2205.
(20) Jiang, N.; Xu, H.; Wang, L.; Jiang, J.; Zhang, T. Nonradical oxidation of pollutants with single-atom-Fe(III)-activated persulfate: Fe(V) being the possible intermediate oxidant. *Environ. Sci. Technol.* **2020**, *54*, 14057−14065.
(21) Wang, Z.; Qiu, W.; Pang, S.; Gao, Y.; Zhou, Y.; Cao, Y.; Jiang, J. Relative contribution of ferryl ion species (Fe(IV)) and sulfate radical formed in nanoscale zero valent iron activated peroxydisulfate and peroxymonosulfate processes. *Water Res.* **2020**, *172*, No. 115504.
(22) Chen, J.; Zhou, X.; Sun, P.; Zhang, Y.; Huang, C.-H. Complexation enhances Cu(II)-activated peroxydisulfate: A novel activation mechanism and Cu(III) contribution. *Environ. Sci. Technol.* **2019**, *53*, 11774−11782.
(23) Wang, L.; Xu, H.; Jiang, N.; Wang, Z.; Jiang, J.; Zhang, T. Trace cupric species triggered decomposition of peroxymonosulfate and degradation of organic pollutants: Cu(III) being the primary and selective intermediate oxidant. *Environ. Sci. Technol.* **2020**, *54*, 4686−4694.
(24) Wang, Y.; Wu, Y.; Yu, Y.; Pan, T.; Li, D.; Lambropoulou, D.; Yang, X. Natural polyphenols enhanced the Cu(II)/peroxymonosulfate (PMS) oxidation: The contribution of Cu(III) and HO•. *Water Res.* **2020**, *186*, No. 116326.
(25) Jawad, A.; Zhan, K.; Wang, H.; Shahzad, A.; Zeng, Z.; Wang, J.; Zhou, X.; Ullah, H.; Chen, Z.; Chen, Z. Tuning of persulfate activation from a free radical to a nonradical pathway through the incorporation of non-redox magnesium oxide. *Environ. Sci. Technol.* **2020**, *54*, 2476−2488.
(26) Zhou, X.; Ke, M. K.; Huang, G. X.; Chen, C.; Chen, W. X.; Liang, K.; Qu, Y. T.; Yang, J.; Wang, Y.; Li, F. T.; Yu, H. Q.; Wu, Y. E. Identification of Fenton-like active Cu sites by heteroatom modulation of electronic density. *Proc. Natl. Acad. Sci. U. S. A.* **2022**, *119*, 2119492119.
(27) Popova, T. V.; Aksenova, N. V. Complexes of copper in unstable oxidation states. *Russ. J. Coord. Chem.* **2003**, *29*, 743−765.
(28) Feng, Y.; Qing, W.; Kong, L.; Li, H.; Wu, D.; Fan, Y.; Lee, P.-H.; Shih, K. Factors and mechanisms that influence the reactivity of trivalent copper: A novel oxidant for selective degradation of antibiotics. *Water Res.* **2019**, *149*, 1−8.
(29) Zhang, T.; Zhu, H.; Croué, J.-P. Production of sulfate radical from peroxymonosulfate induced by a magnetically separable $CuFe_2O_4$ spinel in water: efficiency, stability, and mechanism. *Environ. Sci. Technol.* **2013**, *47*, 2784−2791.
(30) Wang, X.; Li, Y. Rational synthesis of α-MnO_2 single-crystal nanorods. *Chem. Commun.* **2002**, *7*, 764−765.
(31) Hu, P.; Su, H.; Chen, Z.; Yu, C.; Li, Q.; Zhou, B.; Alvarez, P. J. J.; Long, M. Selective degradation of organic pollutants using an efficient metal-free catalyst derived from carbonized polypyrrole via peroxymonosulfate activation. *Environ. Sci. Technol.* **2017**, *51*, 11288−11296.
(32) Wang, Z.; Bush, R. T.; Sullivan, L. A.; Chen, C.; Liu, J. Selective oxidation of arsenite by peroxymonosulfate with high utilization efficiency of oxidant. *Environ. Sci. Technol.* **2014**, *48*, 3978−3985.
(33) Ali, J.; Wenli, L.; Shahzad, A.; Ifthikar, J.; Aregay, G. G.; Shahib, I. I.; Elkhlifi, Z.; Chen, Z.; Chen, Z. Regulating the redox centers of Fe through the enrichment of Mo moiety for persulfate activation: A new strategy to achieve maximum persulfate utilization efficiency. *Water Res.* **2020**, *181*, No. 115862.
(34) Shao, P.; Yu, S.; Duan, X.; Yang, L.; Shi, H.; Ding, L.; Tian, J.; Yang, L.; Luo, X.; Wang, S. Potential difference driving electron transfer via defective carbon nanotubes toward selective oxidation of organic micropollutants. *Environ. Sci. Technol.* **2020**, *54*, 8464−8472.
(35) Shao, P.; Jing, Y.; Duan, X.; Lin, H.; Yang, L.; Ren, W.; Deng, F.; Li, B.; Luo, X.; Wang, S. Revisiting the graphitized nanodiamond-mediated activation of peroxymonosulfate: Singlet oxygenation versus electron transfer. *Environ. Sci. Technol.* **2021**, *55*, 16078−16087.
(36) Qin, J.; Dai, L.; Shi, P.; Fan, J.; Min, Y.; Xu, Q. Rational design of efficient metal-free catalysts for peroxymonosulfate activation: Selective degradation of organic contaminants via a dual nonradical reaction pathway. *J. Hazard. Mater.* **2020**, *398*, No. 122808.
(37) Lim, J.; Yang, Y.; Hoffmann, M. R. Activation of peroxymonosulfate by oxygen vacancies-enriched cobalt-doped black TiO_2 nanotubes for the removal of organic pollutants. *Environ. Sci. Technol.* **2019**, *53*, 6972−6980.
(38) Huang, C.; Wang, Y.; Gong, M.; Wang, W.; Mu, Y.; Hu, Z.-H. α-MnO_2/Palygorskite composite as an effective catalyst for heterogeneous activation of peroxymonosulfate (PMS) for the degradation of Rhodamine B. *Sep. Purif. Technol.* **2020**, *230*, No. 115877.
(39) Chen, X.; Chen, J.; Qiao, X.; Wang, D.; Cai, X. Performance of nano-Co_3O_4/peroxymonosulfate system: Kinetics and mechanism study using Acid Orange 7 as a model compound. *Appl. Catal., B* **2008**, *80*, 116−121.
(40) Deng, Y.; Handoko, A. D.; Du, Y.; Xi, S.; Yeo, B. S. *In situ* Raman spectroscopy of copper and copper oxide surfaces during electrochemical oxygen evolution reaction: identification of Cu^{III} oxides as catalytically active species. *ACS Catal.* **2016**, *6*, 2473−2481.
(41) Xu, J. F.; Ji, W.; Shen, Z. X.; Li, W. S.; Tang, S. H.; Ye, X. R.; Jia, D. Z.; Xin, X. Q. Raman spectra of CuO nanocrystals. *J. Raman Spectrosc.* **1999**, *30*, 413−415.
(42) Bang, J.; Jung, Y.; Kim, H.; Kim, D.; Cho, M.; Ko, S. H. Multi-bandgap monolithic metal nanowire percolation network sensor integration by reversible selective laser-induced redox. *Nano-Micro Lett.* **2022**, *14*, 49.
(43) Henson, M. J.; Mukherjee, P.; Root, D. E.; Stack, T. D. P.; Solomon, E. I. Spectroscopic and electronic structural studies of the $Cu(III)_2$ bis-μ-oxo core and its relation to the side-on peroxo-bridged dimer. *J. Am. Chem. Soc.* **1999**, *121*, 10332−10345.
(44) Ren, D.; Deng, Y.; Handoko, A. D.; Chen, C.; Malkhandi, S.; Yeo, B. S. Selective electrochemical reduction of carbon dioxide to ethylene and ethanol on copper(I) oxide catalysts. *ACS Catal.* **2015**, *5*, 2814−2821.
(45) Schreier, M.; Héroguel, F.; Steier, L.; Ahmad, S.; Luterbacher, J. S.; Mayer, M. T.; Luo, J.; Grätzel, M. Solar conversion of CO_2 to CO using Earth-abundant electrocatalysts prepared by atomic layer modification of CuO. *Nat. Energy* **2017**, *2*, 17087.
(46) Wan, L.; Zhou, Q.; Wang, X.; Wood, T. E.; Wang, L.; Duchesne, P. N.; Guo, J.; Yan, X.; Xia, M.; Li, Y. F.; Jelle, A. A.; Ulmer, U.; Jia, J.; Li, T.; Sun, W.; Ozin, G. A. Cu_2O nanocubes with

https://doi.org/10.1021/acs.est.2c01968
Environ. Sci. Technol. 2022, 56, 8984−8992

mixed oxidation-state facets for (photo)catalytic hydrogenation of carbon dioxide. *Nat. Catal.* **2019**, *2*, 889−898.
(47) Wang, Y.; Xia, H.; Sun, K.; Wu, S.; Lu, W.; Xu, J.; Li, N.; Pei, K.; Zhu, Z.; Chen, W. Insights into the generation of high-valent copper-oxo species in ligand-modulated catalytic system for oxidizing organic pollutants. *Chem. Eng. J.* **2016**, *304*, 1000−1008.
(48) Feng, Y.; Lee, P.-H.; Wu, D.; Shih, K. Surface-bound sulfate radical-dominated degradation of 1,4-dioxane by alumina-supported palladium (Pd/Al_2O_3) catalyzed peroxymonosulfate. *Water Res.* **2017**, *120*, 12−21.
(49) Miao, J.; Geng, W.; Alvarez, P. J. J.; Long, M. 2D N-doped porous carbon derived from polydopamine-coated graphitic carbon nitride for efficient nonradical activation of peroxymonosulfate. *Environ. Sci. Technol.* **2020**, *54*, 8473−8481.
(50) Yang, Y.; Banerjee, G.; Brudvig, G. W.; Kim, J. H.; Pignatello, J. J. Oxidation of organic compounds in water by unactivated peroxymonosulfate. *Environ. Sci. Technol.* **2018**, *52*, 5911−5919.
(51) Huang, M.; Han, Y.; Xiang, W.; Zhong, D.; Wang, C.; Zhou, T.; Wu, X.; Mao, J. In situ-formed phenoxyl radical on the CuO surface triggers efficient persulfate activation for phenol degradation. *Environ. Sci. Technol.* **2021**, *55*, 15361−15370.
(52) Miao, J.; Zhu, Y.; Lang, J.; Zhang, J.; Cheng, S.; Zhou, B.; Zhang, L.; Alvarez, P. J. J.; Long, M. Spin-state-dependent peroxymonosulfate activation of single-atom M−N moieties via a radical-free pathway. *ACS Catal.* **2021**, *11*, 9569−9577.
(53) Spaeth, A. D.; Gagnon, N. L.; Dhar, D.; Yee, G. M.; Tolman, W. B. Determination of the Cu(III)-OH bond distance by resonance raman spectroscopy using a normalized version of Badger's rule. *J. Am. Chem. Soc.* **2017**, *139*, 4477−4485.
(54) Wu, L.; Sun, Z.; Zhen, Y.; Zhu, S.; Yang, C.; Lu, J.; Tian, Y.; Zhong, D.; Ma, J. Oxygen vacancy-induced nonradical degradation of organics: Critical trigger of oxygen (O_2) in the Fe-Co LDH/peroxymonosulfate system. *Environ. Sci. Technol.* **2021**, *55*, 15400−15411.
(55) Shi, Z.; Wang, D.; Gao, Z.; Ji, X.; Zhang, J.; Jin, C. Enhanced ferrate oxidation of organic pollutants in the presence of Cu(II) Ion. *J. Hazard. Mater.* **2022**, *433*, No. 128772.
(56) Hickman, A. J.; Sanford, M. S. High-valent organometallic copper and palladium in catalysis. *Nature* **2012**, *484*, 177−185.
(57) Himes, R. A.; Karlin, K. D. A new copper-oxo player in methane oxidation. *Proc. Natl. Acad. Sci. U. S. A.* **2009**, *106*, 18877−18878.
(58) Bouchey, C. J.; Tolman, W. B. Involvement of a formally copper(III) nitrite complex in proton-coupled electron transfer and nitration of phenols. *Inorg. Chem.* **2022**, *61*, 2662−2668.
(59) Su, H.; Wei, Y.; Qu, X.; Yu, C.; Li, Q.; Alvarez, P. J. J.; Long, M. Mechanistic inference on the reaction kinetics of phenols and anilines in carbon nanotubes-activated peroxydisulfate systems: pp-LFERs and QSARs analyses. *Chem. Eng. J.* **2020**, *385*, No. 123923.
(60) Phipps, R. J.; Gaunt, M. J. A meta-selective copper-catalyzed C-H bond arylation. *Science* **2009**, *323*, 1593−1597.
(61) Larson, V. A.; Battistella, B.; Ray, K.; Lehnert, N.; Nam, W. Iron and manganese oxo complexes, oxo wall and beyond. *Nat. Rev. Chem.* **2020**, *4*, 404−419.
(62) Lee, H.; Lee, H. J.; Seo, J.; Kim, H. E.; Shin, Y. K.; Kim, J. H.; Lee, C. Activation of oxygen and hydrogen peroxide by copper(II) coupled with hydroxylamine for oxidation of organic contaminants. *Environ. Sci. Technol.* **2016**, *50*, 8231−8238.
(63) Tratnyek, P. G.; Hoigne, J. Oxidation of substituted phenols in the environment: A QSAR analysis of rate constants for reaction with singlet oxygen. *Environ. Sci. Technol.* **1991**, *25*, 1596−1604.

https://doi.org/10.1021/acs.est.2c01968
Environ. Sci. Technol. 2022, 56, 8984−8992